ICIC Express Letters
Part B: Applications
Volume **12**, Number **6**, June **2021**

ICIC International ©2021 ISSN 2185-2766
pp. 567–576

QUANTITATIVE EVALUATION OF BRIDGE FLOOR CRACKS BY USING 2-DIMENSIONAL COMPLEX DISCRETE WAVELET PACKET TRANSFORM

Zhong Zhang[1], Takuma Sogabe[2], Takuma Akiduki[2]
Taiki Saito[3] and Kazuhiro Hayashi[3]

[1]Department of Intelligent Mechanical Engineering
Hiroshima Institute of Technology
2-1-1 Miyake, Saeki-ku, Hiroshima 731-5193, Japan
t.sho.g4@cc.it-hiroshima.ac.jp

[2]Department of Mechanical Engineering
[3]Department of Architecture and Civil Engineering
Toyohashi University of Technology
1-1 Hibarigaoka Tenpaku-cho, Toyohashi 441-8580, Japan
akiduki@is.me.tut.ac.jp; tsaito@ace.tut.ac.jp

Received November 2020; accepted January 2021

Abstract. *Bridge floor inspections are usually done visually on site. The evaluations depend on the inspector's skill and place a large burden on the inspector and for these reasons are problematic. To tackle these problems, inspection by image processing technology has been developed in recent years. Automatic evaluation by image processing for bridge floors requires feature quantity extraction of cracks. In this study, we extracted three main crack feature quantities, lengths, directional components, and widths for crack binary images converted from captured images of the bridge floor. Crack length extraction was done using Hilditch thinning and directional component extraction was done using directional selectivity of a two-dimensional complex wavelet packet transform (2D-CWPT). Furthermore, crack width extraction was done by applying reconstruction images for 2D-CWPT and machine learning.*
Keywords: 2D-CWPT, Feature value extraction, Crack, Frequency analysis, Image processing

1. **Introduction.** In the periodic inspection of bridge floors, visual observation of cracks is mainly done by inspectors. The inspectors evaluate the bridge floor condition based on crack feature quantities such as length, direction and width, and the usage environment of the bridge. However, there are problems in that differences in evaluation occur based on the inspector's skill level and a large burden is placed on the inspector, with long work hours and dangers in the work environment. To solve these problems, inspection by image processing technology for quantitative evaluation and reduction of the inspector's burden has been developed in recent years [1, 2, 3, 4, 5, 6, 7].

The 2D-CWPT is one crack analysis method for bridge floor images, which is fit for inspecting sharp edges [8, 9]. This method analyzes images into frequency components by calculating wavelet packet coefficients, which are degrees of correlation between image brightness and a wavelet, which is a wave with a specific shape. The 2D-CWPT can analyze frequency components in more detail than the conventional discrete wavelet transform (DWT) and has translation invariance, which is invariance of detection accuracy regardless of position changes. Therefore, the 2D-CWPT is suitable for high-accuracy crack detection and can create binary images of cracks extracted from captured images of bridge floors. A captured image and a crack binary image are shown in Figures 1(a)

DOI: 10.24507/icicelb.12.06.567

(a) Captured image (b) Binary image

FIGURE 1. Crack detection for bridge floors

and 1(b), respectively. For quantitative evaluation of bridge floors by image processing, feature value extraction of cracks from binary images as in Figure 1(b) is needed.

In this study, the extracted crack feature values were lengths, directional components and widths, and methods to extract these feature values from crack binary images were examined. The remainder of the paper is organized as follows: In Section 2, the principle and characteristic of the 2D-CWPT are introduced; Section 3 details extraction methods of crack lengths; Section 4 is concerned with extraction methods of crack directional components; Section 5 explains extraction methods of crack widths and considers the results. Finally, Section 6 gives conclusions and closing remarks.

2. **Review of the Two-Dimensional Complex Wavelet Packet Transform (2D-CWPT).** The complex discrete wavelet transform (CDWT) is compatible with the conventional discrete wavelet transform (DWT), with the additional property that the signal can be completely reconstructed by high-speed processing and conversion, or inverse transformations [10, 11]. A mother wavelet (MW) of the CDWT is constituted by two orthogonal wavelets with real part $\psi^R(x)$ and imaginary part $\psi^I(x)$. Further, the scaling function also has a real $\phi^R(x)$ and an imaginary $\phi^I(x)$ part. In the time domain, the positions of the real and imaginary parts are shifted 1/2 sample towards each other, and this produces the conditions for translation invariance in the complex wavelet. The CWPT is a method of producing improved frequency resolution of the CDWT [12] and the 2D-CWPT is a two-dimensional extension of the CWPT [13]. The 2D-CWPT, therefore, is able to analyze detailed frequency components, unlike the conventional 2D-CDWT. This means that the 2D-CWPT has improved resolution of directional selectivity.

The 2D-CDWT, like the 2D-CWPT, can analyze a two-dimensional signal using the scaling function and the MW with real and imaginary parts. However, the 2D-CWPT does not distinguish between the wavelet coefficients of the high-frequency component and scaling coefficients of the low-frequency component, and therefore, all of the coefficients are recursively filtered by the 2D-CWPT. Moreover, each wavelet packet coefficient obtained by the 2D-CWPT in each analysis level (frequency band) is classified by the index (n, m) as shown in Figure 2, where Figure 2(a) shows decomposition level $j = -1$, and Figure 2(b) shows decomposition level $j = -2$. In the figures, all the frequency components are divided into three major areas, in which the components of the region of $\max(n, m) = 2$ are defined as the low-frequency components (orange color), the components of the region of $\max(n, m) = 3$ are defined as the intermediate-frequency components (blue color), and the components of the region of $\max(n, m) = 4$ are defined as the high-frequency components (pink color).

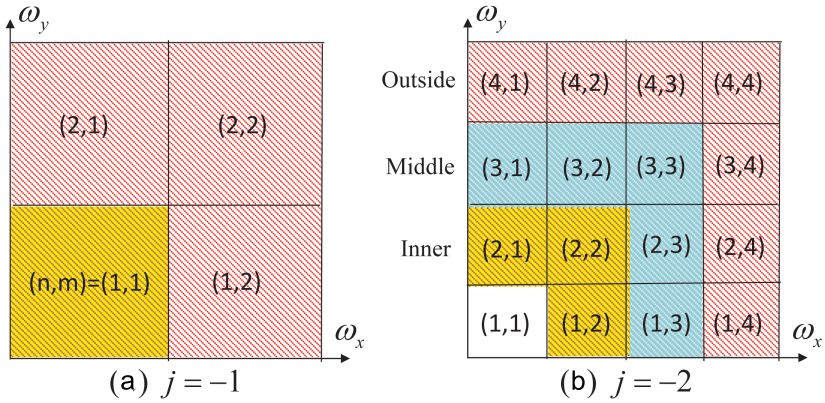

FIGURE 2. (color online) The index of each frequency component

In the figure, n represents the vertical direction of the frequency component ω_y, and m represents the horizontal direction of the frequency component ω_x. If n and m are small numbers, they represent a low frequency component. On the contrary, if n and m are large numbers, they represent a high frequency component.

Further, the analysis level 0 index $(1,1)$ of the wavelet packet coefficient is expressed as $d_{0,k_x,k_y}^{RI,(1,1)}$. This is equal to the scaling coefficient c_{0,k_x,k_y}^{RI} of the conventional CDWT, and is given by Equation (1).

$$d_{0,k_x,k_y}^{RI,(1,1)} = c_{0,k_x,k_y}^{RI}, \tag{1}$$

where k_x, k_y show the position coordinate of the wavelet coefficient corresponding to the horizontal frequency ω_x and the vertical frequency ω_y, respectively. The other wavelet packet coefficients $d_{0,k_x,k_y}^{RR,(1,1)}$, $d_{0,k_x,k_y}^{IR,(1,1)}$, $d_{0,k_x,k_y}^{II,(1,1)}$ are derived in the same way. In addition, the wavelet packet coefficients vary in accordance with the analytical level and index. Besides this, the directional components are given by Equations (2)-(7).

$$D_{j,n_x,n_y}^{R0,(n,m)} = \frac{d_{j,n_x,n_y}^{RR,(n,m)} + d_{j,n_x,n_y}^{II,(n,m)}}{2}, \tag{2}$$

$$D_{j,n_x,n_y}^{I0,(n,m)} = \frac{d_{j,n_x,n_y}^{IR,(n,m)} - d_{j,n_x,n_y}^{RI,(n,m)}}{2}, \tag{3}$$

$$D_{j,n_x,n_y}^{R1,(n,m)} = \frac{d_{j,n_x,n_y}^{RR,(n,m)} - d_{j,n_x,n_y}^{II,(n,m)}}{2}, \tag{4}$$

$$D_{j,n_x,n_y}^{I1,(n,m)} = \frac{d_{j,n_x,n_y}^{IR,(n,m)} + d_{j,n_x,n_y}^{RI,(n,m)}}{2}, \tag{5}$$

$$\left|D_{j,n_x,n_y}^{0,(n,m)}\right| = \sqrt{\left(D_{j,n_x,n_y}^{R0,(n,m)}\right)^2 + \left(D_{j,n_x,n_y}^{I0,(n,m)}\right)^2}, \tag{6}$$

$$\left|D_{j,n_x,n_y}^{1,(n,m)}\right| = \sqrt{\left(D_{j,n_x,n_y}^{R1,(n,m)}\right)^2 + \left(D_{j,n_x,n_y}^{I1,(n,m)}\right)^2}. \tag{7}$$

Calculations using Equations (2)-(7) are performed in each of indexes (n,m). In addition, $\left|D_{j,n_x,n_y}^{0,(n,m)}\right|$, $\left|D_{j,n_x,n_y}^{1,(n,m)}\right|$, and the like are AVDC (absolute values of directional components).

Figure 3 shows $\left|D_{j,n_x,n_y}^{0,(n,m)}\right|$, $\left|D_{j,n_x,n_y}^{1,(n,m)}\right|$ obtained by Equations (6) and (7), and placed according to each frequency component. Figure 4 shows directional components that correspond to $\left|D_{j,n_x,n_y}^{0,(n,m)}\right|$, $\left|D_{j,n_x,n_y}^{1,(n,m)}\right|$ shown in Figure 3. It can be seen from Figure 4 that the 2D-CWPT of decomposition level $j=-2$ extracts 14 directional components in the

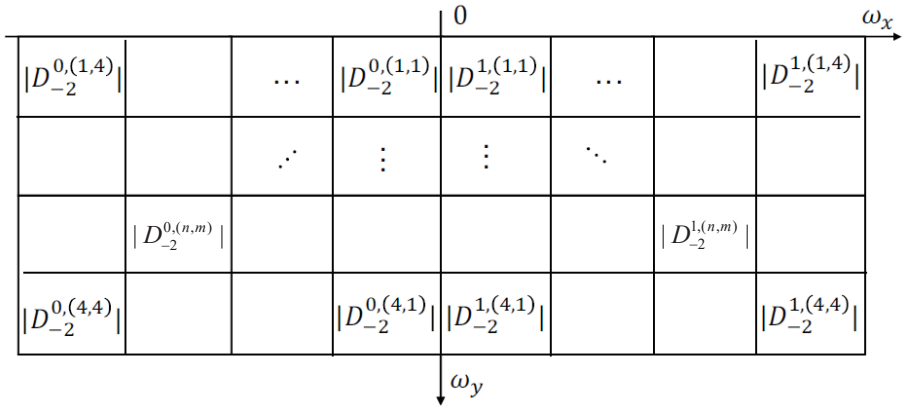

FIGURE 3. The location of each frequency component in 2D-CWPT

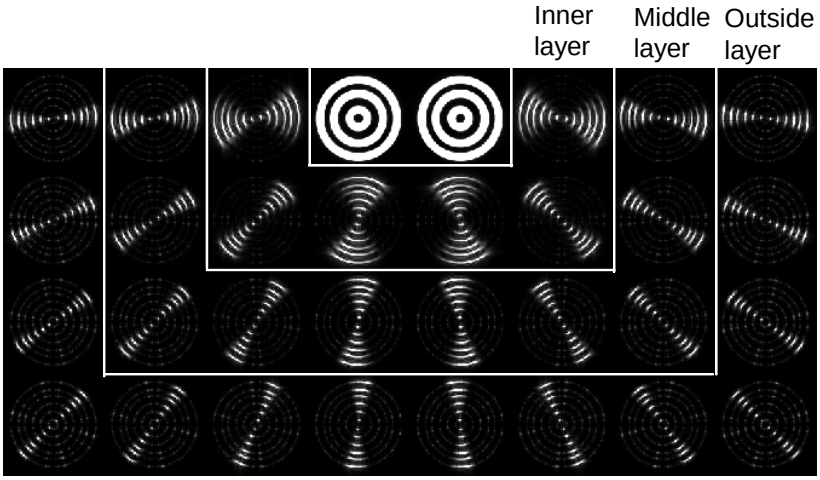

FIGURE 4. The result of directional selection of 2D-CWPT using model image

outside layer, 10 directional components in the middle layer, and 6 directional components in the inner layer, respectively.

For quantitative evaluation of bridge floors, the edge extraction of cracks was done using crack binary image obtained from the 2D-CWPT crack detection [9]. Furthermore, extracted feature values also include lengths, directional components and widths. Lengths and widths are generally utilized as evaluation factors of concrete structures [4, 5]. Directional components have been found to be an important factor to evaluate slipperiness regarding load applied to bridge floors [2]. In the following sections, new methods to extract each feature value by using the 2D-CWPT will be explained and the results are considered.

3. **Length Extraction of Cracks.** The Hilditch thinning algorithm was performed as a preprocessing step of length extraction [1]. It converts objects in images into line segments having 8-neighbor connectivity and 1 pixel width by means of sequential conversions of foreground pixels applying the following conditions into background pixels.

- **Condition 1**: Being a foreground pixel

$$B(P_0) = 1. \tag{8}$$

- **Condition 2**: Being a boundary pixel

$$\sum_{k \ni N_{odd}} \{1 - |B(P_k)|\} \geq 1. \tag{9}$$

- **Condition 3**: Not deleting end pixels

$$\sum_{k \ni N_8} |B(P_k)| \geq 2. \tag{10}$$

- **Condition 4**: Not deleting isolated pixels

$$\sum_{k \ni N_8} C_k \geq 1, \quad C_k = \begin{cases} 1 & (B(P_k) = 1) \\ 0 & (B(P_k) \neq 1) \end{cases}. \tag{11}$$

- **Condition 5**: Holding connectivities

$$\begin{aligned} &N_C^8(P_0) = 1 \text{ where} \\ &N_C^8(P_0) = \sum_{k \ni N_{odd}} D(P_k)\{1 - D(P_{k+1})D(P_{k+2})\}, \\ &D(P_k) = 1 - B(P_k). \end{aligned} \tag{12}$$

- **Condition 6**: Deleting only one side pixel of line segments having 2 pixel width. Applying either of following conditions for all of n $(n = 0 \sim 8)$

$$\begin{aligned} &(i)\, B(P_n) \neq 1 \\ &(ii)\, B(P_n) = 0 \text{ than } N_C^8 = 1. \end{aligned} \tag{13}$$

However, the target pixel is P_0, 8-neighbor pixels of the target pixel are $P_1, \ldots, P_8$, the pixel value of P_i $(= 0 \sim 8)$ is represented as $G(P_i)$, the background pixel value is 0 and the foreground pixel value is 1. In addition, $N_8 = \{P_1, \ldots, P_8\}$, $N_{odd} = \{P_1, P_3, P_5, P_7\}$ are defined. Each of the binary images before and after Hilditch thinning are shown in Figure 5(a) and Figure 5(b), respectively. In Figure 5(a), circled numbers represent crack labels.

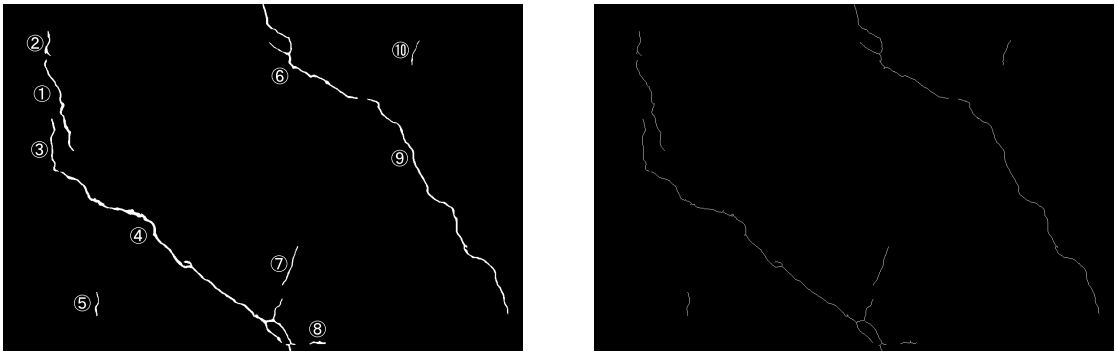

(a) Binary image (b) Thinning image

FIGURE 5. Hilditch thinning algorithm

For each of the cracks in Figure 5(b), lengths were calculated by the following equation.

$$L_i = \sum_{k=1}^{C} d_k. \tag{14}$$

However, L_i is the crack length of label i, C is the summation of the connections, d is the Euclidean distance between the centers of connected pixels, and k is the connection index. Extracted lengths of each of the cracks are shown in Table 1.

In Figure 5 and Table 1, it can be confirmed that calculated crack lengths are in proportion to the actual lengths and consistent with the relative lengths of each crack.

TABLE 1. Results of crack length extraction

Crack labels	Crack lengths [px]	Crack labels	Crack lengths [px]
1	252	6	441
2	73	7	105
3	140	8	46
4	973	9	695
5	60	10	65

4. **Directional Component Extraction of Cracks.** In the 2D-CWPT, it has been confirmed that there are correlations between frequency characteristics of wavelet and directions of edge detection [13]. Therefore, arbitrary directional components in images can be extracted by applying low pass or high pass filters to the conventional 2D-CWPT. Directional components are calculated from AVDC as explained in Section 2 and Equations (15)-(21).

$$F_{D,2}^{R,H} = \sum_{k_y} D_{2,n_x,k_y}^{R0,(m,n)} DF_{l_1}^{H}(n_y - k_y), \tag{15}$$

$$F_{D,2}^{I,H} = \sum_{k_y} D_{2,n_x,k_y}^{I0,(m,n)} DF_{l_1}^{H}(n_y - k_y), \tag{16}$$

$$F_{D,2}^{R,L} = \sum_{k_y} D_{2,n_x,k_y}^{R0,(m,n)} DF_{l_2}^{L}(n_y - k_y), \tag{17}$$

$$F_{D,2}^{I,L} = \sum_{k_y} D_{2,n_x,k_y}^{I0,(m,n)} DF_{l_2}^{L}(n_y - k_y), \tag{18}$$

$$AF_D^H = \sqrt{\left(F_D^{R,H}\right)^2 + \left(F_D^{I,H}\right)^2}, \tag{19}$$

$$AF_D^L = \sqrt{\left(F_D^{R,L}\right)^2 + \left(F_D^{I,L}\right)^2}, \tag{20}$$

$$AF_D^{\theta_1\theta_2} = AF_D^H + AF_D^L. \tag{21}$$

However, (n, m), shown in Figure 3, are indexes to represent frequency domains containing extraction directions, $DF_{l_1}^H$ and $DF_{l_2}^L$ are low pass or high pass filters. Furthermore, $AF_D^{\theta_1\theta_2}$ is defined as the directional component in the range $\theta_1 \sim \theta_2$.

In this study, directional components of each of the cracks in the range of 45 degrees, centered on the 4 directions of 0, 45, 90, 135 degrees were extracted. The histograms of directional components of the extracted cracks of labels 4, 7 and 9 in Figure 5(a) are shown in Figure 6, respectively. However, crack elongation directions are orthogonal to extraction directions because the crack directional components are edge intensity values detected for extraction directions.

In Figure 6, it can be confirmed that 4 directional components are obtained for each crack. As an example, it is presumed from Figure 6(a) that the crack of label 4 is extended in the 135-degree direction because the 45-degree component is the largest and inclines to the horizontal direction because the 90-degree component is larger than the 0-degree component. Thus, the crack elongation direction is presumed quantitatively from the relative value of each of directional components.

5. **Width Extraction of Cracks.** The 2D-CWPT can create reconstructed images having only specific frequency components by leaving only the wavelet packet coefficients of arbitrary frequency domain and deleting the other coefficients. Frequency components of

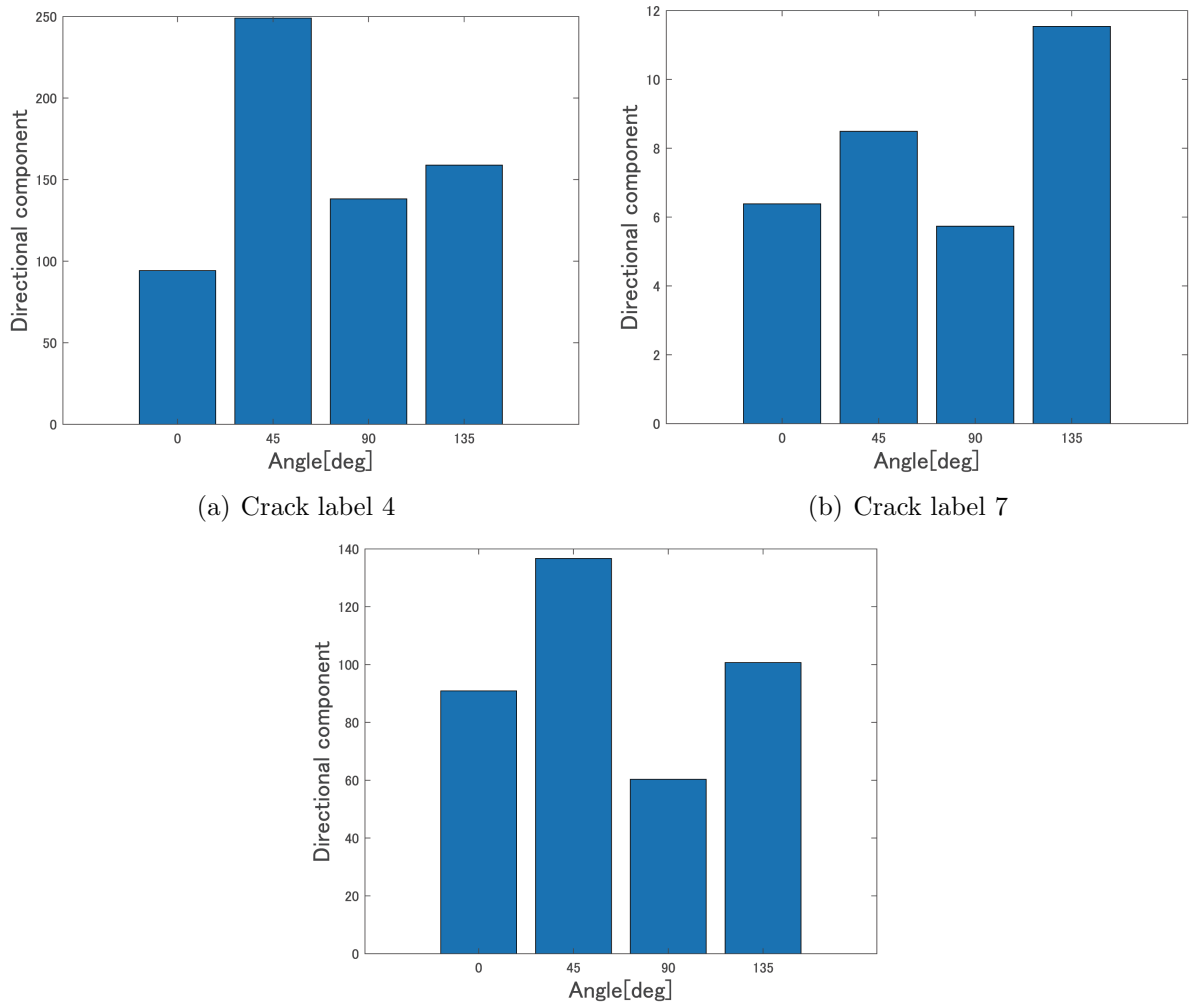

(a) Crack label 4

(b) Crack label 7

(c) Crack label 9

FIGURE 6. Directional components

cracks in the images depend on their widths. In reconstructed images, correlation values corresponding to crack widths can be obtained as brightness values because peaks in brightness values appear largely in the area correlated to each frequency domain. As examples, model image imitated cracks and reconstructed images are shown in Figure 7(a) and Figures 7(b)-7(d), respectively. In Figure 7(a), line segments having $1, 2, \ldots, 10$ pixel widths are drawn from the left side at a certain interval. Besides this, Figure 7(b) represents low frequency components, Figure 7(c) represents intermediate frequency components and Figure 7(d) represents high frequency components. From Figures 7(b)-7(d), it is confirmed that different brightness values are obtained for each width and frequency component.

For the extraction method of crack widths, a 2D-CWPT of decomposition level $j = -4$ converted 25 crack binary images into 16 layers of reconstructed images per image. In only 4 low frequency layers of the reconstructed images, containing remarkable brightness peaks on cracks, brightness values were extracted as factors for crack width classification. In addition, a dataset containing the classification factors and correct labels of crack widths obtained from benchmark images was created. Crack width extraction by classifiers and the dataset was carried out. However, 3 classifiers, namely a decision tree, a k-nearest neighbor classifier (k-NN) and a support vector machine (SVM), were utilized for comparison of accuracy. Configuration of the extraction system is shown in Figure 8.

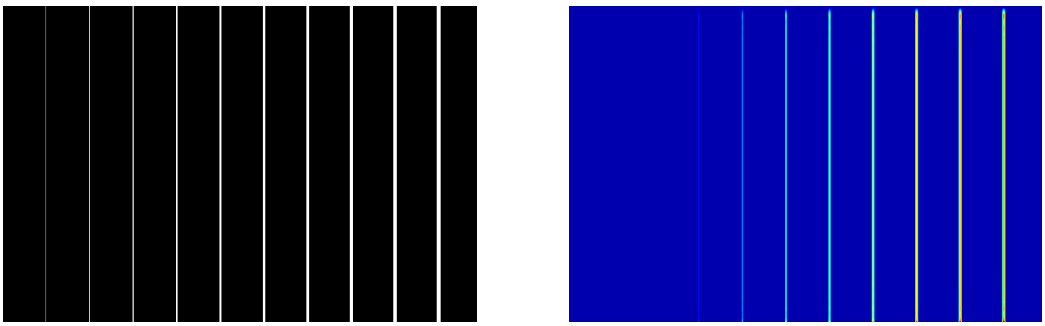

(a) Model crack image

(b) Low frequency image

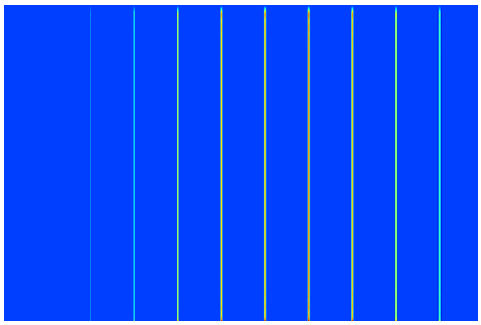

(c) Intermediate frequency image

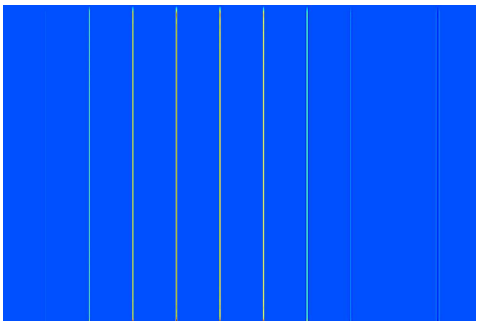

(d) High frequency image

FIGURE 7. Reconstruction by 2D-CWPT

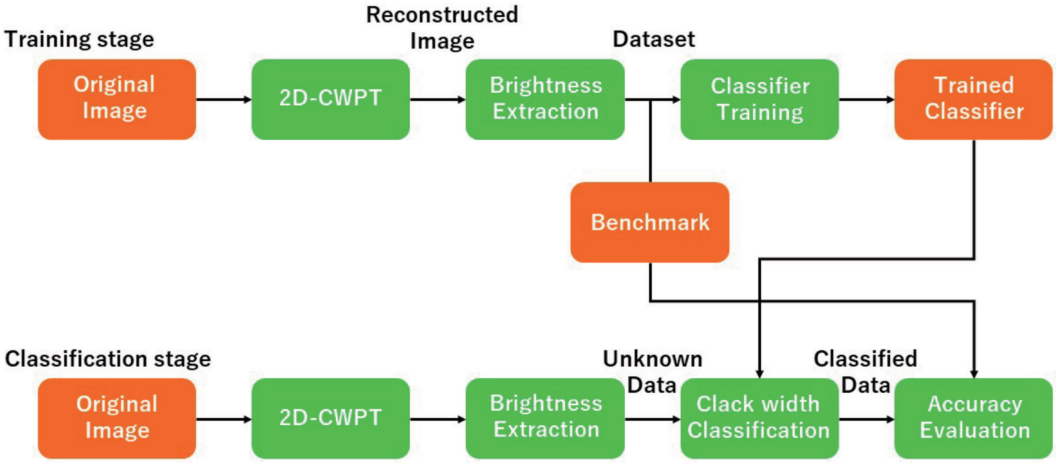

FIGURE 8. System architecture

TABLE 2. Accuracy and classification speed for crack width measurement

Classifier	Accuracy [%]	Classification speed [point/sec]
Decision tree	54.6	500000
k-NN	59.1	26000
SVM	60.7	250

Accuracies were calculated by 10-fold cross-validation utilized generally for classifier accuracy validation. The accuracies and classification speeds are shown in Table 2.

In Table 2, it is shown that the SVM achieved the highest accuracy of 60.7% and the SVM was optimal in terms of accuracy. However, the SVM is mainly utilized in 2 class

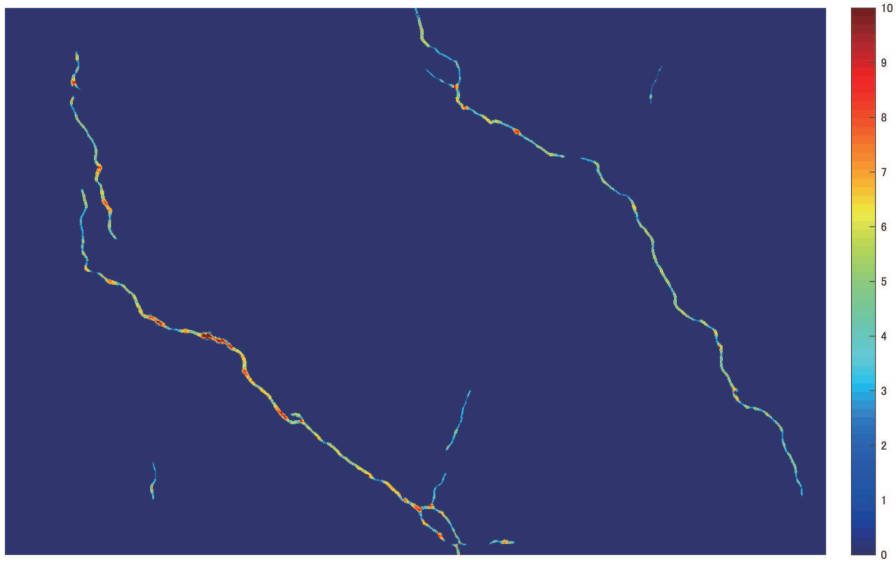

FIGURE 9. (color online) Extracted crack width image

classification and needs to be combined with several SVMs. Therefore, its calculation costs are higher than the other classifiers. As a result, its classification speed is also slow. For this reason, in the case of analyzing a large number of images, the decision tree or k-NN is more suitable because of their high classification speed. Besides this, a crack image containing extracted crack widths as brightness values is shown in Figure 9. In Figure 9, it is confirmed that the extraction system can obtain values corresponding to crack widths.

6. **Conclusion and Remarks.** To construct a quantitative evaluation system for bridge floors by image processing, extraction of crack lengths, directional components and widths was carried out. The results obtained are as follows.

1) Crack lengths were extracted by applying Hilditch thinning. As a result, values corresponding to the crack lengths were obtained.
2) Crack directional components were obtained by 2D-CWPT directional selectivity and shown in histograms. Crack elongation directions can be presumed from relative differences between directional components.
3) Crack widths were extracted by means of brightness values of 2D-CWPT reconstructed images and machine learning. The highest accuracy was 60.7% in the case where an SVM was utilized as a classifier.

Research on the extraction of features of cracks in concrete structures is being actively conducted, especially in companies. Although there are few precedents for the extraction of directional components, many extraction methods have been proposed for the length and width. In order to evaluate the superiority of each proposed method in this study, therefore, it is necessary to evaluate the extraction accuracy by comparing it with those extraction methods using a large number of sample images.

Acknowledgment. This work was partially supported by JSPS KAKENHI Grant Numbers 16H03143 and 19H02223. The authors also gratefully acknowledge the helpful comments and suggestions of the reviewers.

REFERENCES

[1] H. Yashida, N. Tanaka and T. Inoue, On misuse of the connectivity condition in the Hilditch thinning algorithm, *The Journal of the Institute of Image Electronics Engineering of Japan*, vol.39, no.4, pp.490-493, 2000 (in Japanese with English Abstract).

[2] Y. Shigeta, T. Tobita, K. Kamemura, M. Shinji, I. Yoshitake and K. Nakagawa, Proposal of tunnel crack index (TCI) as an evaluation method for lining concrete, *Journal of Japan Society of Civil Engineers F*, vol.62, no.4, pp.628-632, 2006 (in Japanese with English Abstract).
[3] T. C. Hutchinson and Z. Q. Chen, Improved image analysis for evaluating concrete damage, *Journal of Computing in Civil Engineering*, vol.20, no.3, pp.2010-2016, 2006.
[4] Y. Fujita, H. Nakamura and Y. Hamamoto, Classification of crack width of concrete structure by image processing, *Proc. of the Japan Concrete Institute*, vol.34, no.1, pp.1792-1797, 2012 (in Japanese).
[5] S. Kushiyama, Study on measuring of concrete crack length for RC buildings using image processing, *Bulletin of the Faculty of Engineering Hokkai-Gakuen University*, vol.40, pp.19-31, 2017 (in Japanese).
[6] L. Guo, R. Li, B. Jiang and X. Shen, Automatic crack distress classification from concrete surface images using a novel deep-width network architecture, *Neurocomputing*, vol.397, pp.383-392, 2020.
[7] Y. Shin, M. Kim, K.-W. Pak and D. Kim, Practical methods of image data preprocessing for enhancing the performance of deep learning based road crack detection, *ICIC Express Letters, Part B: Applications*, vol.11, no.4, pp.373-379, 2020.
[8] Z. Zhang, O. Hamada, H. Toda, T. Akiduki and T. Miyake, Bridge floor cracks detection by using the 2 dimensional complex discrete wavelet packet transform, *Proc. of the 2016 International Conference on Wavelet Analysis and Pattern Recognition (ICWAPR2016)*, pp.225-229, 2016.
[9] Z. Zhang, O. Hamata, T. Akiduki, T. Mashimo, T. Saito and K. Hayashi, Cracks in bridge floor detected by 2 dimensional complex discrete wavelet packet transform, *International Journal of Innovative Computing, Information and Control*, vol.16, no.6, pp.2007-2019, 2020.
[10] N. G. Kingsbury, The dual-tree complex wavelet transform: A new technique for shift invariance and directional filters, *IEEE Dgital Signal Processing Workshop (DSP2013)*, pp.2543-2560, 1998.
[11] H. Toda and Z. Zhang, Perfect translation invariance with a wide range of shapes of Hilbert transform pairs of wavelet bases, *International Journal of Wavelets, Multiresolution and Information Processing*, vol.8, no.4, pp.501-520, 2010.
[12] H. Toda, Z. Zhang and T. Imamura, The design of complex wavelet packet transforms based on perfect translation invariance theorems, *International Journal of Wavelets, Multiresolution and Information Processing*, vol.8, no.4, pp.537-558, 2010.
[13] T. Kato, Z. Zhang, H. Toda, T. Imamura and T. Miyake, A novel design method for directional selection based on 2-dimensional complex wavelet packert transform, *International Journal of Wavelets, Multiresolution and Information Processing*, vol.11, no.4, 2013.